frontiers | Frontiers in Earth Science

TYPE Original Research
PUBLISHED 07 September 2023
DOI 10.3389/feart.2023.1255712

OPEN ACCESS

EDITED BY
Ryan Mathur,
Juniata College, United States

REVIEWED BY
Pura Alfonso,
Universitat Politecnica de Catalunya, Spain
Maciej Manecki,
AGH University of Science and Technology, Poland

*CORRESPONDENCE
Paolo Fulignati,
paolo.fulignati@unipi.it
Maurizio Mulas,
mmulas@espol.edu.ec

†These authors share first authorship

RECEIVED 09 July 2023
ACCEPTED 28 August 2023
PUBLISHED 07 September 2023

CITATION
Fulignati P, Mulas M, Villalta Echeverria MDP, Fornasaro S, Larreta E, Mendoza Arteaga PL, Menoscal Menoscal MA, Romero-Crespo P and Gioncada A (2023), The propylitic alteration in the Ponce Enriquez Gold Mining district, Azuay province, Ecuador: genetic constraints from a mineral chemistry and fluid inclusions study.
Front. Earth Sci. 11:1255712.
doi: 10.3389/feart.2023.1255712

The propylitic alteration in the Ponce Enriquez Gold Mining district, Azuay province, Ecuador: genetic constraints from a mineral chemistry and fluid inclusions study

Paolo Fulignati[1]*†, Maurizio Mulas[2]*†, Michelle Del Pilar Villalta Echeverria[2], Silvia Fornasaro[1], Erwin Larreta[2,3], Pierina Lisbeth Mendoza Arteaga[2], Melanie Annabela Menoscal Menoscal[2], Paola Romero-Crespo[2] and Anna Gioncada[1]

[1]Dipartimento di Scienze della Terra, University of Pisa, Pisa, Italy, [2]Escuela Superior Politécnica del Litoral, ESPOL, Facultad de Ingeniería en Ciencias de la Tierra, Guayaquil, Ecuador, [3]Instituto de Investigación Geológico Energético (IIGE), Quito, Ecuador

Wide areas of the Southern sector of Ecuador are characterized by Cretaceous mafic volcanic rocks, pervasively altered by a propylitic mineralogical assemblage with epidote, chlorite, and quartz with minor titanite, illite and prehnite. These propylitically altered rocks host significant gold mineralization in veins, deeply exploited in the last decades. Porphyry Au-Cu deposits also occur in the area. This work focuses on the study of this propylitic alteration to assess the genetic conditions and the relation with the distance from the porphyry system, through the chemical composition of the secondary minerals (particularly trace elements in epidote and chlorite) and fluid inclusion data. The aim is to improve knowledge of the trace element geochemistry of secondary minerals in propylitic alteration and their relationship to the causative porphyry systems. The results of this work indicate that alteration affecting the rocks of the Pallatanga Fm. can be related to the propylitic hydrothermal alteration halo of porphyry copper deposits. Fluid inclusion investigation in quartz veins associated with epidote and chlorite evidenced at least two pulses of hydrothermal fluids characterized by temperature around 345°C for the first one and around 305°C for the second one. The salinity of the fluids is always low (around 1.5 wt % $NaCl_{equiv.}$) suggesting a dominantly meteoric component. Evidence of boiling processes have not been observed. We hypothesize that the hydrothermally altered "green rocks" of the Ponce Enriquez Mining District could be envisaged as the propylitic halo of the Miocene hornblende-bearing Au-Cu porphyry deposits of Gaby-Papa Grande, and discuss the epidote and chlorite trace element composition in this scenario. The results help improving the general knowledge of the propylitically altered rocks in southern Ecuador and add new data for the use of trace element chemistry of epidote and chlorite in mineral exploration elsewhere.

KEYWORDS

propylitic alteration, epidote, chlorite, fluid inclusions, Ponce Enriquez Mining district

1 Introduction

Propylitic alteration, as a distal alteration zone of porphyry-centered hydrothermal systems, has been traditionally considered poor of useful information for mineral exploration. Therefore, the controls on the formation of this alteration facies have not been studied in depth since a few years ago. However, several recent papers demonstrated that the trace element composition of epidote and chlorite has significant potential to provide spatial compositional trends useful for mineral exploration (i.e., vectoring toward mineralized/hydrothermal centers within propylitically altered terrain, differentiate propylitic alteration around ore deposits from the similar assemblages developed during regional metamorphism), because they are able to record the dispersion of many elements as a consequence of changing physicochemical conditions across the propylitic facies (Cooke et al., 2014; Wilkinson et al., 2015; Cooke et al., 2020a; Ahmed et al., 2020; Baker et al., 2020; Cooke et al., 2020b; Pacey et al., 2020; Wilkinson et al., 2020; Li et al., 2022). In this scenario, data on the mineral chemistry of propylitic alteration minerals related to ore deposits worldwide are needed, to improve understanding of this widespread and still incompletely studied alteration style.

These features are clearly exposed in southern Ecuador where the metallogenic belts, dating to Jurassic and to Tertiary times, host notable Au, Cu, Mo, and Ag resources (PRODEMINCA, 2000; Schutte et al., 2010; Schutte et al., 2012). In the Ponce Enriquez Mining District (PEMD hereafter), the Cretaceous tholeiitic basalts of Pallatanga Formation (Fm.), covered by Miocene ignimbrites, are intruded by Miocene Au-porphyries and host an important gold mineralization. These mafic rocks are deeply altered by a mineralogical assemblage dominated by the occurrence of chlorite and epidote. The Ponce Enriquez gold mineralization is not well known. The environmental implications linked to the mining activity in the area have been tackled in several works (PRODEMINCA, 2000; Appleton et al., 2001; Carling et al., 2013; Pesantes et al., 2019; Jiménez-Oyola et al., 2021a; Jiménez-Oyola et al., 2021b), but the fluid evolution, the mechanisms that control the formation of this huge gold mineralization hosted within "green rocks," the relationship between the mineralization and the propylitic alteration, and the possible relationships with the nearby porphyry systems are not still fully reconstructed.

In this paper, we present a case study concerning the propylitic alteration of PEMD, focusing on the trace element chemical composition of the secondary minerals (particularly epidote and chlorite) and on fluid inclusion data. The aim is to shed light on the fluid evolution and conditions that led the development of propylitic alteration, and on the possible relationships with the occurrence of porphyry systems only few hundreds of meters far. The results help improving the knowledge of the "green rocks" in the southern Ecuador, opening the possibility to employ the epidote and chlorite chemistry as a tool in mineral exploration to assess the relationships to causative porphyry systems. Moreover, we add new data for understanding the formation of propylitic alteration style and for using trace element chemistry of epidote and chlorite in mineral exploration elsewhere.

2 Geological background

The PEMD (Azuay Province) is sited in southern Ecuador on the western flank of the Western Cordillera and is comprised between two hydrographic basins: the Río Siete basin to the south and the Río Guanache basin to the north (Figure 1). The Pallatanga Fm., the Yunguilla Fm., and the Saraguro Group (Las Trancas Fm.) outcrop in this area (Figure 1) (PRODEMINCA, 2000). The Pallatanga Fm. (Cretaceous) corresponds to an ophiolitic association, and it is composed of a sequence of oceanic basalts, pillow lavas, hyaloclastites, and massive dolerites with aphanitic and variolitic textures (Kerr et al., 2002; Srivastava et al., 2008). The material presents geochemical features of accreted igneous oceanic terranes that include calc-alkaline material of an island arc sequence, and oceanic plateau material (Kerr et al., 2002). Most of the rocks of the Pallatanga Fm. are aphanitic, but locally these are enriched in phenocrysts of pyroxene and plagioclase and locally small gabbroid bodies occur inside the main body. From the geochemical point of view, the main rocks of the Pallatanga Fm. are basalt with a SiO_2 content varying from 47% to 53% and MgO from 7% to 9% and tholeiitic affinity (Kerr et al., 2002). With regard to the trace elements, they have high concentrations in Y, Nb and V. The La/Yb ratio is low (<2.5), the Zr/Th ratio is >200 while the chondrite-normalized REE show flat patterns (Kerr et al., 2002).

The Yunguilla Fm. (Upper Cretaceous, Maastrichtian) corresponds to a turbidite fan sequence made up of siltstones, feldspathic quartz-type sandstones, and quartz arenites (Duque, 2000). According to Thalmann (1946), this formation is more than 1,000 m thick.

The Saraguro Group (Late Eocene—Early Miocene) is mainly composed of welded ignimbrites and lavas interbedded with sedimentary rocks (Siravo et al., 2021). It is divided into two main sequences: the lower sequence (Portovelo Unit and Las Trancas Fm.), composed of quartz-diorites and granodiorites/tonalites (Egüez et al., 2017), and the upper sequence (Plancharumi, La Fortuna, Jubones, and La Paz Fm.), made up of rhyolitic ignimbrites (PRODEMINCA, 2000). The Portovelo Unit is composed of andesitic to basaltic lavas and andesitic ignimbrites that outcrop north of the Piñas-Portovelo Fault. The Las Trancas Fm. (Oligocene) sited at southwest of PEMD, lies on the Pallatanga Fm. and it is composed of andesitic to dacitic ignimbrites, conglomerates, argillites, and feldspars, muscovite, and quartz-rich sandstones (PRODEMINCA, 2000). The Plancharumi Fm. (Oligocene) is made up of stratified rhyolitic ignimbrites, rhyolitic breccias, and lavas interbedded with ash, sandstone, and claystone (Dunkley and Gaibor, 1997). The La Fortuna Fm. (Early Miocene) is located northward of the Jubones Fault and is composed by aphyric ignimbrites. It reaches a maximum thickness of 600 m (Pratt et al., 1997). The Jubones Fm. (Early Miocene) represents the top of the Saraguro Group, and it can reach 500 m of thickness (Hungerbühler, 1997). It is a rhyolitic welded ignimbrite rich in quartz, biotite, and plagioclase crystals. The Saraguro Group presents multiple Tertiary intrusions, and it hosts several epithermal deposits of Miocene age that make up the Azuay and El Oro districts (PRODEMINCA, 2000; Schutte et al., 2012).

In the PEMD, porphyry Cu (Chaucha) and porphyry Au-Cu deposits (Gaby-Papa Grande) are related with the large Oligocene to Miocene intrusive centers. The Gaby-Papa Grande hornblende

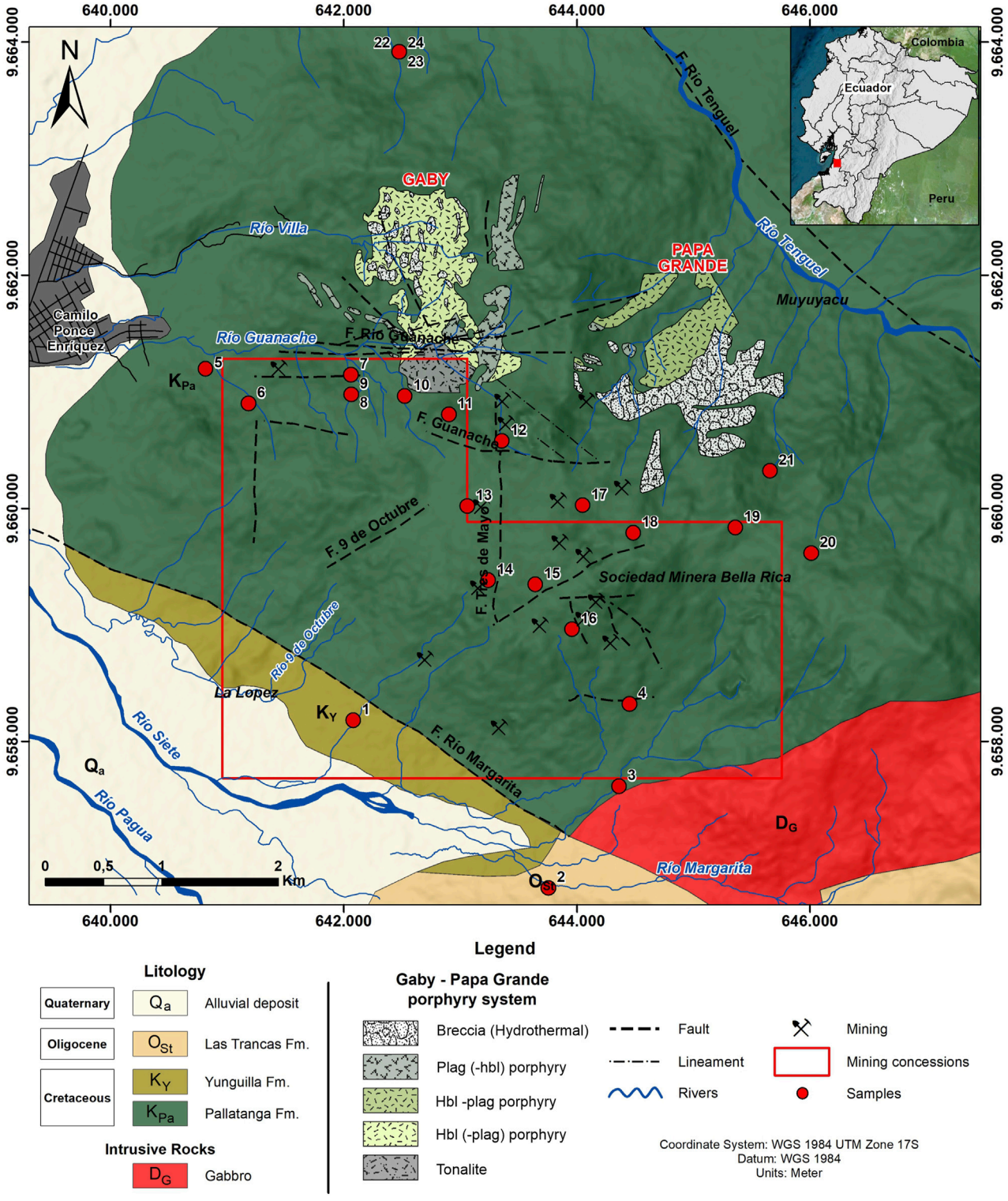

FIGURE 1
Geologic map of Ponce Enriquez mining district showing the location of the studied samples.

Au-Cu porphyry (20.54 ± 0.08 million years, Schutte et al., 2012) is located to the north of Bella Rica Mining Cooperative (Figure 1). It is intruded in Cretaceous mafic volcanic rocks and shows euhedral hornblende and plagioclase phenocrysts. The rocks outcropping around these porphyry intrusions belong to the Pallatanga Fm. and mostly consist of dark greenish-gray basaltic andesites with aphanitic texture and andesites with a porphyritic texture with millimeter-sized or close to a centimeter plagioclase phenocrysts

with breccias, veins, and mineralization in stockwork (PRODEMINCA, 2000).

In the PEMD sector, different fault systems with a N-S, NW-SE, or WNW-ESE orientation (Figure 1) of Cenozoic age (PRODEMINCA, 2000) are present. In the northeast of Ponce Enríquez, the Tenguel River Fault is present while in the southwest the Margarita Fault divides the Bella Rica basalts (Pallatanga Fm.) from the turbiditic sediments (Yunguilla Fm.) The Guanache Fault is north dipping (50°–80°), parallel to the Guanache River (Figure 1) and the Eloy Calderón vein is located in correspondence of this fault (Dunkley and Gaibor, 1997). The other main fault system presents an E-W and NE-SW directions. The Los Ratones Fault has dips between 60° and 90° to the NW; in the NE sector, a mineralized fault is observed in the Muyuyacu sector. The Río 9 de Octubre Fault tilts to the SE and it extends to the Papa Grande porphyritic complex (PRODEMINCA, 2000). Here the mineralized veins show E-W strike direction. The mineralized Tres de Mayo Fault presents a N-S direction, and it dips to the east displaced by the regional transversal faults. In general, the hydrothermal mineralization in the Bella Rica area is N-S oriented on transverse fault structures and east-dipping veins due to an existing paleosuture. Minerals such as pyrrhotite, pyrite, galena, hematite, sphalerite, chalcopyrite, magnetite, molybdenite, calcite, chlorite, among others, have been identified (AMBIENCONSUL, 2017).

3 Materials and methods

Twenty-one rock samples were collected in the area of the Bella Rica Mining Cooperative and in the northern side of the area (Figure 1). Thirty-one thin sections were prepared in the Petrography Laboratory of the Engineering in Earth Sciences (FICT) of the Polytechnic University of Litoral (ESPOL) of Guayaquil, Ecuador. Polished thin sections for reflected light optical microscopy, scanning electron microscopy - backscattered electron imaging (SEM-BSEI), electron probe micro-analyzer (EPMA), and Laser Ablation Inductively Coupled Plasma Mass Spectrometry (LA-ICPMS) analysis were prepared in the laboratories of the Earth Science Department of Pisa, Italy.

Bulk rock geochemistry was carried out on 10 samples on pulps obtained by crushing in a jaw mill and pulverized in agate jars rock chips picked out of macroscopically visible quartz and sulfide veins, to gain information on the propylitically altered host rock. Major element composition and Loss On Ignition (LOI) were determined at Actlabs (Canada) by the Inductively Coupled Plasma Optical Emission Spectrometry (ICP-OES) technique using the Varian 720-ES. Bulk rock trace elements were determined after HNO_3-HF acid-digestion by means of a Perkin-Elmer NexION 300x ICP-MS at Earth Science Department of Pisa.

FE-SEM-EDS analyses were performed using the FEI Quanta FEG 450 apparatus housed at the Centre for Instrument Sharing of University of Pisa (CISUP). The EPMA analyses of chlorite, epidote, feldspar, and amphibole were performed on carbon-coated and polished thin sections, using a JEOL JXA-8200 Super-Probe at the Earth Sciences Department Ardito Desio, University of Milan, Italy. Operating conditions were 15 kV and a beam current of 5 nA. The instrument is equipped with five wavelength-dispersive spectrometers (WDS) with a range of LiF, PET and TAP crystals, and one additional EDS detector, and was internally calibrated using mineral standards and metals of natural and synthetic origin, notably: grossular (Si Kα, Ca Kα, Al Kα), omphacite (Na Kα), forsterite (Mg Kα), fayalite (Fe Kα), ilmenite (Ti Kα), orthoclase (K Kα), rhodonite (Mn Kα), pure metal Cr (Cr Kα). Raw element data were ZAF-corrected using a phi-rho-Z analysis program, and corrected element contents were converted to oxide contents in weight percent (wt%) assuming stoichiometry. FeO_{tot} represents total iron (oxide) content.

In-situ trace element analyses on epidote and chlorite, previously analyzed by means of EPMA, were performed by laser ablation inductively coupled plasma mass spectrometry (LA-ICPMS). The LA-ICPMS analyses were performed using a PerkinElmer NexION 2000 ICP-MS coupled with a New Wave Research-193 Ar-F 193 nm excimer laser, at the Earth Science Department of Pisa, in the laboratories of the Centre for Instrument Sharing of University of Pisa (CISUP). The laser was operated at a repetition rate of 10 Hz using spot sizes of 35 and 40 μm and a 4.6 J/cm^2 energy density. Synthetic standard glass NIST 612 was used for external calibration. The accuracy of the analyses was monitored using the synthetic standard glass NIST 610 and CaO and SiO_2 was used as internal standards for epidote and chlorite respectively. Data reduction was performed with the software package IOLITE (Paton et al., 2011). Edges of grains were carefully avoided to ensure no contamination of the analyses occurred due to accidental ablation of adjacent minerals.

Doubly polished thin sections (100–300 μm-thick) were prepared for petrography and microthermometric determinations of fluid inclusions. Fluid inclusion analyses were carried out using a Linkam THMS 600 heating-freezing stage at the Earth Sciences Department of the University of Pisa. The accuracy of measurements is estimated at ±2°C at 398°C controlled by the melting point of $K_2Cr_2O_7$, ±0.1°C at 0°C and ±0.2°C at −56.6°C controlled by using certified pure water and CO_2-bearing synthetic fluid inclusions (Synthetic Fluid Inclusion Reference Set, Bubbles Inc., United States). Salinities of fluid inclusions, expressed in weight percent equivalent NaCl, were calculated from final ice-melting temperature, using the equation of Bodnar (1993) for the H_2O-NaCl system. Eutectic temperature (when observable) was used to constrain overall composition of trapped fluids by comparison with published data for various salt-water systems (Crawford, 1981).

4 Results

4.1 Rock classification

The rocks outcropping in the study area belong to the Pallatanga Fm. and Yunguilla Fm. From a petrographic point of view, they can be classified as basaltic lavas, with porphyritic or aphanitic texture. The phenocrysts, when recognizable, are plagioclase and olivine. The matrix shows spherulitic texture, locally axiolitic, with the classic radial and fibrous aspect of the crystals (Figure 2A). Occasionally, these rocks are aphanitic with allotriomorphic crystals of epidote and quartz and axiolitic spherulitic structures partially chloritized. Three differ, being hornblende-plagioclase-

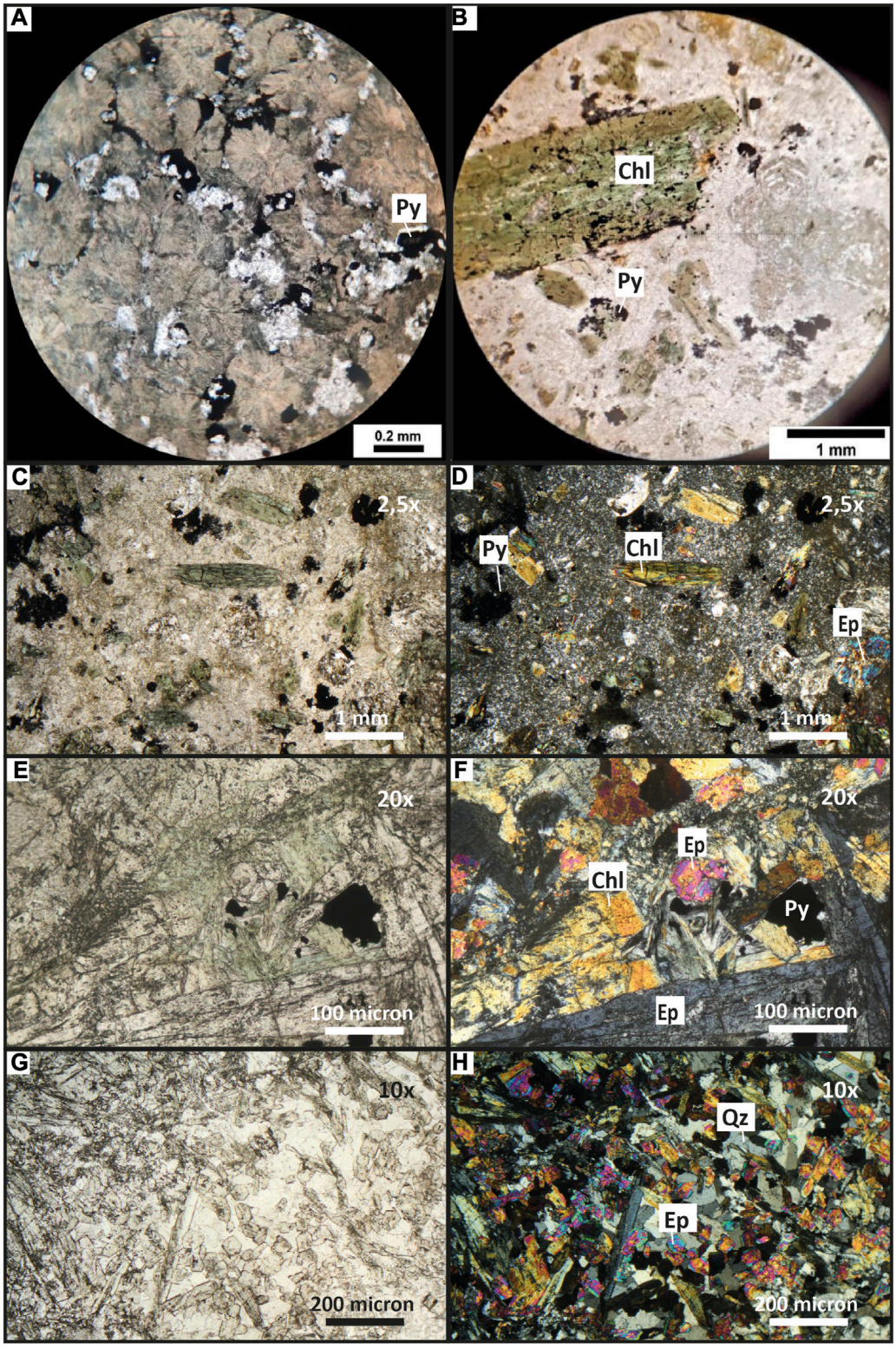

FIGURE 2
Petrographic microphotos of the PEMD propylitically altered Pallatanga lavas with spherulitic texture **(A)** and the porphyritic andesite outcrops **(B–D)**. E, F, G, H: Examples of the propylitic mineral assemblage, dominated by chlorite, epidote and quartz. Parallel **(A–C–E–G)** and crossed nicols **(B–D–F–H)**. Py: pyrite; Chl: Chlorite; Ep: Epidote; Qz: Quartz.

10.3389/feart.2023.1255712

TABLE 1 Major (wt%) and trace elements (ppm) in the PEMD propylitically altered rocks. LOI: loss on ignition.

Sample	PE-01	PE-03	PE-06	PE-07	PE-10	PE-13C	PE-15	PE-16	PE-18	PE-19
SiO_2	49.31	50.18	51.31	60.08	50.36	51.04	48.62	48.99	51.69	48.05
Al_2O_3	14.10	12.63	13.89	16.47	14.47	14.12	12.79	12.19	13.41	12.78
Fe_2O_3(T)	12.55	12.93	10.80	6.03	11.75	11.88	14.11	15.44	12.13	13.9
MnO	0.18	0.18	0.18	0.11	0.19	0.25	0.20	0.22	0.21	0.15
MgO	7.71	6.33	6.89	3.19	7.77	7.46	8.34	10.11	6.44	5.58
CaO	10.60	11.09	8.67	6.11	9.90	5.67	11.71	3.78	9.42	7.35
Na_2O	2.11	2.18	4.16	4.20	2.82	1.90	1.77	0.48	3.67	1.02
K_2O	0.05	0.20	0.07	0.16	0.26	0.06	0.09	0.04	0.11	0.06
TiO_2	0.98	1.19	0.84	0.57	1.00	0.99	0.89	0.90	1.22	1.46
P_2O_5	0.07	0.10	0.07	0.11	0.08	0.08	0.07	0.07	0.11	0.12
LOI	2.65	3.15	2.63	2.27	1.73	6.48	2.05	8.34	2.10	10.37
Li	6.80	9.40	4.80	4.70	4.90	13.70	4.60	25.10	4,00	12.8
Be	0.26	0.30	0.23	0.59	0.24	0.23	0.22	0.21	0.34	0.39
V	331	381	303	154	327	318	305	299	366	374
Cr	231	101	189	53	232	225	212	212	111	113
Co	43	41	37	28	38	40	39	27	45	40
Ni	102	77	96	15	103	102	97	89	83	84
Cu	122	147	61	122	94	116	22	191	207	151
Zn	80	91	76	40	93	1,358	54	163	80	87
Ga	14.6	14.6	15.4	15.6	14.4	14.2	15.3	13.8	15.1	14.9
Rb	0.42	3.79	0.28	3.66	5.93	0.71	1.41	1.38	1.12	2.98
Sr	84	75	126	242	81	61	80	14.5	100	94
Y	23.7	24.8	19.6	16.9	21.2	22	20.6	16.5	25.2	24.9
Zr	48	57	41	43	45	45	41	40	38	66
Nb	3.20	4.10	2.93	2.91	3.30	3.20	3.10	2.93	4.10	4.10
Mo	bdl	Bdl	bdl	bdl	bdl	bdl	bdl	bdl	bdl	bdl
Ag	0.26	0.31	0.20	0.31	0.40	0.46	0.19	0.65	0.22	0.32
Cd	bdl	Bdl	bdl	bdl	0.50	4.62	bdl	0.34	bdl	bdl
Sn	0.51	0.58	0.45	0.36	0.58	0.53	0.59	0.77	0.56	0.61
Sb	bdl	3.50	1.12	bdl	8.90	18.00	19.70	6.90	bdl	3.70
Cs	0.11	0.28	0.07	0.39	1.17	1.54	0.96	1.15	0.30	4.55
Ba	12.7	9.7	25.8	118.0	21.7	16.0	8.2	2.8	21.8	31.0
La	2.84	3.40	2.51	6.40	2.58	3.10	2.69	1.98	3.43	3.50
Ce	7.0	9.0	6.4	13.6	6.9	8.1	6.9	5.3	9.0	9.5
Pr	1.14	1.43	1.01	1.93	1.11	1.27	1.08	0.83	1.41	1.52
Nd	5.7	7.4	5.2	8.6	5.8	6.4	5.6	4.3	7.2	7.8
Sm	1.93	2.48	1.74	2.16	1.99	2.15	1.87	1.50	2.44	2.58
Eu	0.75	0.93	0.79	0.71	0.82	0.84	0.95	0.53	0.96	0.89

(Continued on following page)

TABLE 1 (*Continued*) Major (wt%) and trace elements (ppm) in the PEMD propylitically altered rocks. LOI: loss on ignition.

Sample	PE-01	PE-03	PE-06	PE-07	PE-10	PE-13C	PE-15	PE-16	PE-18	PE-19
Gd	2.80	3.33	2.49	2.47	2.74	2.98	2.63	2.05	3.37	3.43
Tb	0.54	0.64	0.46	0.44	0.53	0.55	0.50	0.41	0.64	0.65
Dy	3.60	4.30	3.14	2.73	3.50	3.70	3.40	2.76	4.30	4.30
Ho	0.82	0.94	0.71	0.60	0.79	0.81	0.77	0.62	0.94	0.97
Er	2.57	2.88	2.19	1.82	2.35	2.53	2.33	1.95	2.81	2.88
Tm	0.38	0.43	0.31	0.26	0.35	0.36	0.33	0.28	0.41	0.42
Yb	2.32	2.62	1.92	1.66	2.23	2.27	2.10	1.84	2.54	2.71
Lu	0.36	0.41	0.31	0.25	0.34	0.35	0.33	0.29	0.40	0.41
Hf	1.41	1.70	1.27	1.27	1.37	1.38	1.25	1.23	1.34	2.02
Ta	0.22	0.27	0.20	0.20	0.22	0.22	0.24	0.20	0.26	0.30
W	bdl	Bdl	Bdl	bdl	0.54	0.63	0.83	bdl	bdl	bdl
Pb	bdl	Bdl	Bdl	bdl	bdl	3.11	bdl	bdl	bdl	bdl
Th	0.24	0.29	0.21	0.93	0.24	0.24	0.20	0.21	0.26	0.30
U	0.07	0.08	0.06	0.29	0.07	0.07	0.07	0.06	0.09	0.09
Th/Ta	1.08	1.08	1.01	1.06	1.10	4.53	1.05	1.09	0.97	0.84
Ba/Nb	4.00	6.66	7.17	2.36	5.01	40.46	0.97	8.80	5.28	2.67
La/Nb	0.89	0.79	0.81	0.82	0.97	2.21	0.68	0.86	0.83	0.87

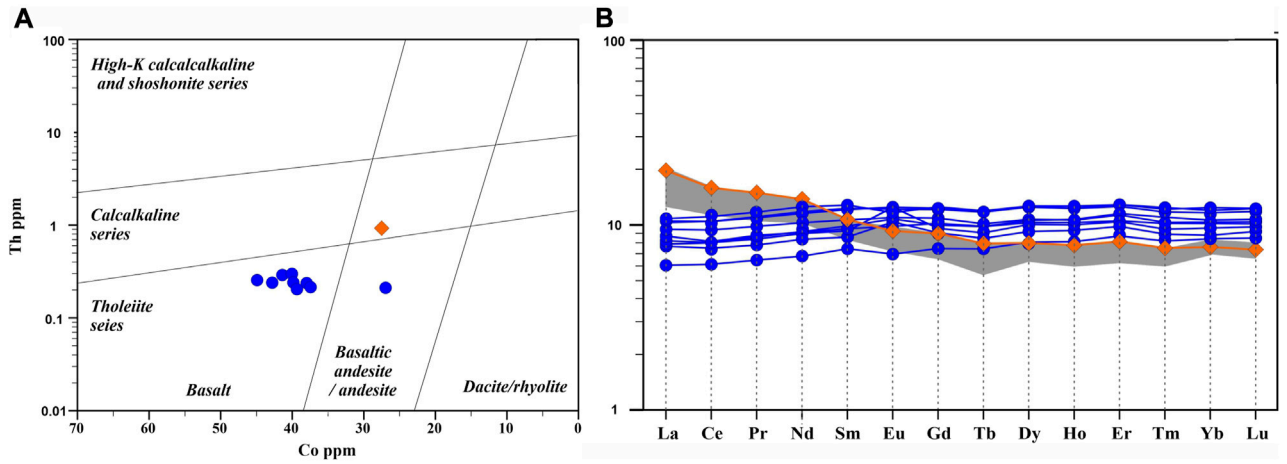

FIGURE 3
(A) Th-Co classification diagram of PEMD altered volcanic rocks (Hastie et al., 2007). **(B)** Chondrite-normalized REE patterns of PEMD altered volcanic rocks. Blue dots: mafic lavas of the Pallatanga Fm; orange diamond: PE-7 andesite sample; gray area: Gaby-Papa Grande porphyry stocks (Schutte et al., 2010).

porphyritic rocks with a medium-grained groundmass and a lower color index, suggesting an intermediate degree of differentiation (PE-7, PE-8, PE-9; see PE-7 in Figures 2B–D). The crystals are subhedral/euhedral with a maximum size of 1.5 mm. Plagioclase crystals are partially obliterated by pervasive alteration. One is made of amphibole (30%), plagioclase (20%), and feldspar (10%) and another one has similar mineralogical composition but it shows higher level of chloritization.

The high LOI of analyzed rocks, above 3% for most samples (Table 1), excludes the classification in the TAS diagram (Le Bas et al., 1986). The geochemical classification of the studied rocks was carried out by using the Th-Co discrimination diagram proposed by Hastie et al. (2007) for the classification of altered volcanic rocks. On the basis of this diagram, all the samples are classified as subalkaline basalts of the tholeiitic series, except for one sample being an andesite of the calc-alkaline series (Figure 3A). The trace

10.3389/feart.2023.1255712

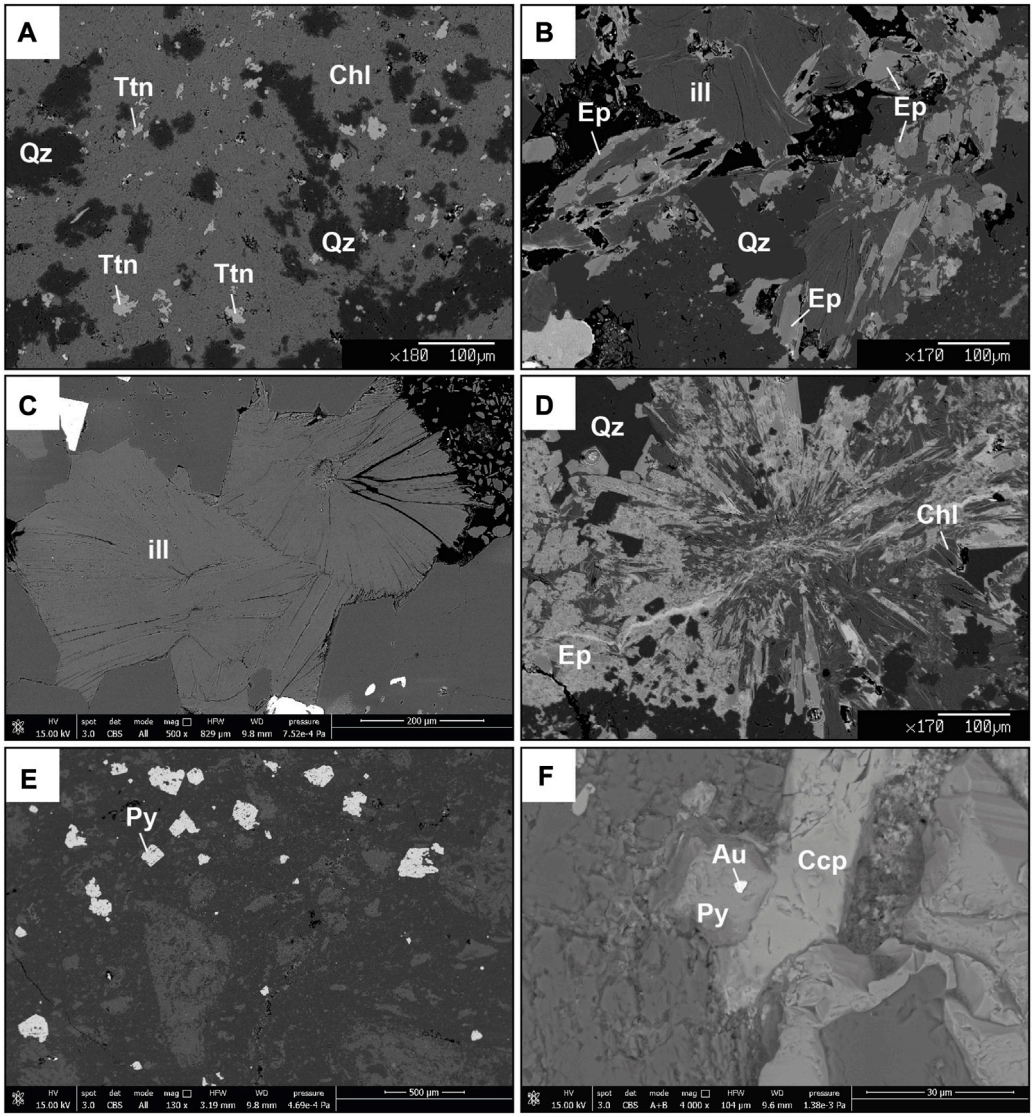

FIGURE 4
Scanning electron microscope BSE images. **(A)** Pervasive propylitic alteration, made up of quartz + chlorite + titanite, obliterates the primary mineralogical assemblage of tholeiitic basalt of Pallatanga Fm. **(B)** Propylitic alteration mineralogical assemblage made up of quartz + chlorite + epidote. **(C)** Crystalline illite found in the propylitic mineralogical assemblage of PE-16 sample. **(D)** Vein of quartz + chlorite + epidote. **(E)** Pyrite crystals in the breccia matrix of brecciated portions of propylitically altered rocks. **(F)** Gold grain found within pyrite in the PE-24 quartz vein. Py: pyrite; Ccp: Calcopyrite; Chl: Chlorite; Ep: Epidote; Qz: Quartz; Au: Gold; Ttn: Titanite; Ill: Illite.

elements normalized to the primitive mantle reveal MORB-like features for the basaltic lavas, while the andesite shows significantly higher Th/Ta, Ba/Nb, and La/Nb ratios, typical of calc-alkaline rocks (Table 1). Accordingly, the REE patterns clearly distinguish the calc-alkaline rock from the other samples (tholeiitic basalts) for the higher La/Sm and La/Yb ratios (Figure 3B).

4.2 Propylitic alteration

The basaltic lavas of Pallatanga Fm. show an intense propylitic alteration consisting of the assemblage chlorite, + epidote + quartz + titanite + sulfides ± illite ± calcite ± prehnite (Figures 2E–H; Figures 4A, B). Illite is found in only one sample (Figure 4C). Adularia is rarely found, not associated with epidote and chlorite, only in hornblende-plagioclase-porphyritic dyke sample. The chemical composition of the propylitic assemblage minerals epidote, chlorite, titanite and illite, as well as of adularia, are reported in the Supplementary Tables S1.

Alteration is pervasive. Veins of quartz associated with epidote and chlorite crosscut the host rock (Figures 2, 4D), which locally shows brecciated portions with sulfides concentrated in the breccia matrix (Figure 4E). Similar hydrothermal mineral assemblages developed in adjacent wall rocks, whose original texture is almost completely destroyed, suggesting that fluids significantly infiltrated in wall rocks along microfractures. The sulfides are dominantly pyrite, disseminated with the propylitic alteration, and arsenopyrite, with minor chalcopyrite, galena, and scarce sphalerite, mostly

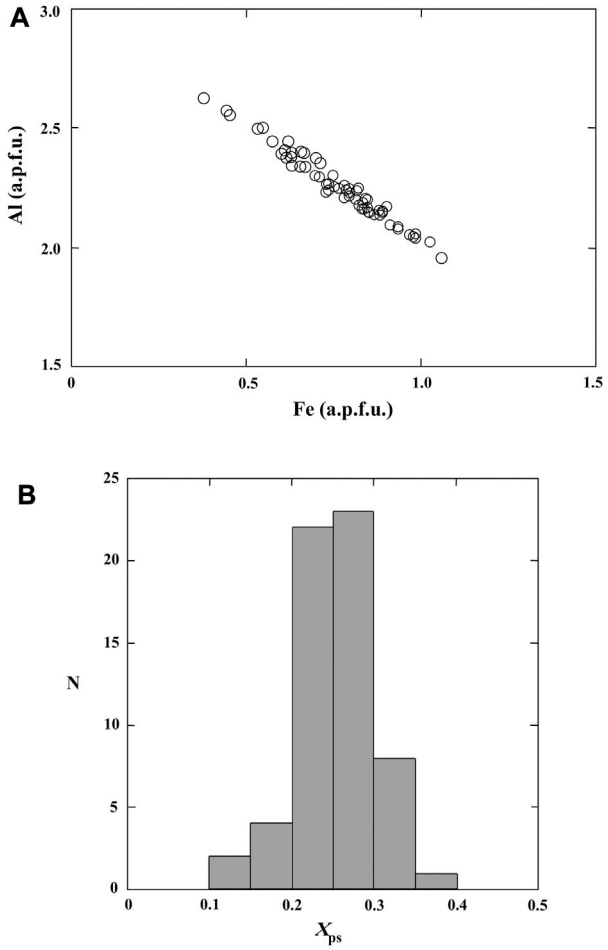

FIGURE 5
Epidote. **(A)** Relationship between iron and aluminum content in epidotes of PEMD. **(B)** Histogram of the pistacite content (Xps) of analyzed epidotes. Data in Supplementary Material S1.

concentrated in veins with quartz ± calcite. Locally, pyrrhotite and cobaltite have been found. In some cases, fracture-filling quartz veins cross-cutting the propylitic assemblage bear gold, electrum, and Au-Ag tellurides as small particles of a few microns (Figure 4F).

4.2.1 Epidote

Major element compositions of the analyzed epidote correspond to true epidote, with a systematic inverse correlation between Fe and Al representing compositions along the epidote-clinozoisite solid solution (Figure 5A). The pistacite content (Xps) of the analyzed epidote spans between 0.13 and 0.35 with a strong mode around 0.25 (Figure 5B). Xps values of the studied epidote crystals fall in the range of hydrothermal epidote found in several active geothermal systems (Cavarretta et al., 1982; Bird et al., 1984; Boyce et al., 2003).

Trace element content of epidote shows that Mn, Sr, V, As and to a lesser extent Zn and Pb are the most abundant (Figure 6), with concentrations exceeding 100 ppm (1,000 ppm in the case of Mn). Antimony is generally below 10 ppm but in a couple of samples it reaches values in excess of 100 ppm (Figure 6). Copper, Bi, Sn, Co, Y, and REE mostly occur in the 0.01–30 ppm range (Figure 6). REE concentration in some cases is however below detection limit. Au, Tl, U, and Th always occur in very low concentration and are often below detection limit.

4.2.2 Chlorite

Major element compositions of chlorites indicate that most of them are pure chlorite. Mixed layers chlorite/smectite (C/S) were only found in a sample, subordinate to pure chlorite and characterized by very high Fe content (up to 50 wt%), and in a gold-bearing quartz vein, as the only phyllosilicate identified. According to Bettison and Schiffman (1988), the mixed layers C/S was distinguished from pure chlorite for their higher number of interlayer cations (Na + K + Ca >0.10 cations apfu/28 Ox), and for a greater amount of Si(IV) cations (>6.25 cations apfu/28 Ox) (Figure 7). Based on the calculated atomic abundances of Fe and Si per formula unit, the chlorite analyzed can be classified as pycnochlorite and ripidolite, having Fe ranging between 3.22 and 5.23 apfu/28 Ox and Si between 5.10 and 6.05 apfu/28 Ox.

LA-ICPMS analyses of chlorite reveal high concentration (tens to thousands ppm) of Mn, Zn, V, Co, Sr, and Ga (Figure 8). These results are consistent with the findings from other case studies of propylitic alteration of porphyry copper deposits (Wilkinson et al., 2015; Wilkinson et al., 2020; Cooke et al., 2020), and are to be ascribed to the substitution of these elements in the structure of chlorite (Wilkinson et al., 2020). Other trace elements found with lower concentration (<10 ppm) are Cu, Sn, Pb, Sb, As, Ba, Y, and REE. Gold, Tl, Bi, U, and Th are generally found in very low concentration and are often below detection limits. As proposed by Wilkinson et al. (2015), the Ti/Sr ratio chlorite proximitor was applied to the composition of the analyzed chlorites and a potential distance ranging from 1,300 to 1,600 m of the samples from the porphyry copper was determined. Using the parameters of chlorite proximitor proposed by Wilkinson et al. (2020) for El Teniente porphyry copper deposit, higher potential distance from the porphyry copper, ranging from 2,050 to 3,600 m was calculated.

Chlorite composition is used to calculate the crystallization temperature by means of the empirical geothermometers of Cathelineau (1988) and Jowett (1991), which are based on the observed systematic increase of Al(IV) content of chlorite with increasing temperature. Both geothermometers gave similar results, showing crystallization temperatures ranging between 252°C and 373°C, with a strong mode at about 315°C (Figure 9).

4.2.3 Illite

Illite was only found in one sample. It appears well crystallized, and the analyses reveal a partial filling of the interlayer site (Na + Ca + K = 1.50–1.68 apfu/22 Ox), and relatively high Fe content (up to 5.25 wt%). This latter reflect the substitution of Fe (phengitic component) for Al in octahedral position according to the substitution: (Fe^{2+}, Mg) VI + (Si^{4+}) IV = (Al^{3+}) IV + (Al^{3+}) VI, typical of illites (Fulignati, 2020 and reference therein).

4.3 Fluid inclusions

Fluid inclusions were found hosted in quartz crystals in veins with epidote and were classified according to phase types at room temperature. All descriptions refer to fluid inclusion assemblages (FIAs). A FIA represents a group of fluid inclusions that, based on

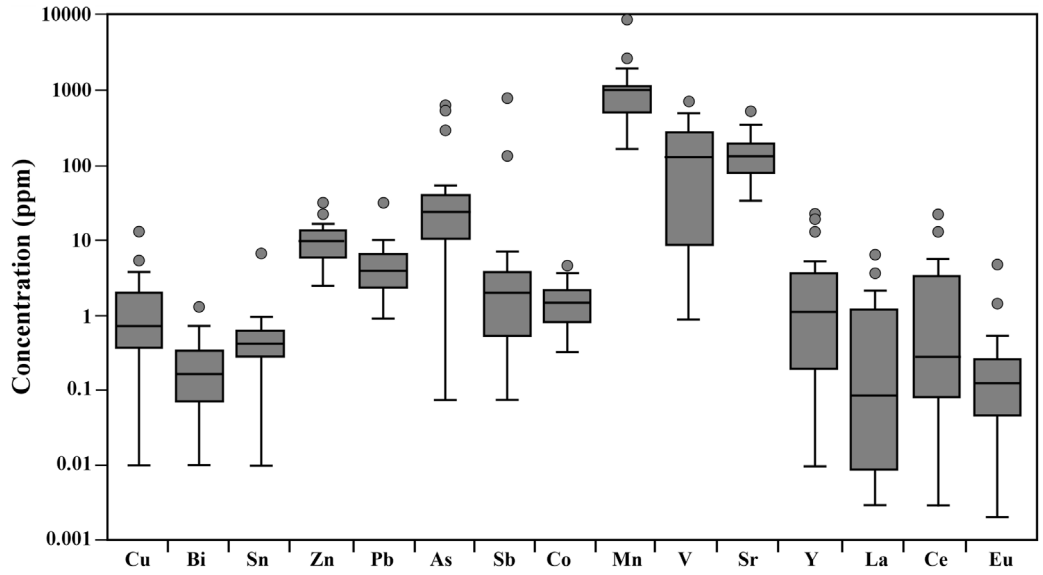

FIGURE 6
Summary of compositional ranges of selected minor and trace elements in epidote from PEMD. Horizontal line represents median; box represents 25th to 75th percentiles, whiskers represent maximum and minimum excluding outliers; circles represent outliers. Data in Supplementary Material S1.

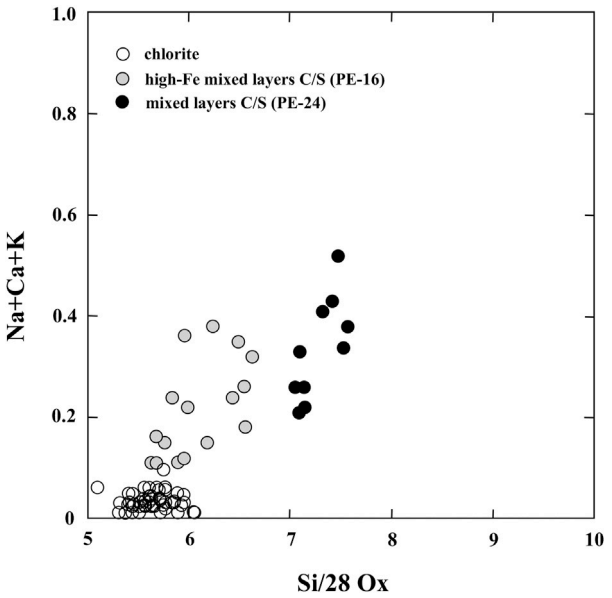

FIGURE 7
Sum of interlayer cations (Na + Ca + K) versus Si content of chlorite and mixed layers C/S. All analyses recalculated on a 28 Ox basis. Data in Supplementary Material S1.

petrography, were all trapped at the same time (Goldstein and Reynolds, 1994). Most FIAs observed in quartz crystals from Ponce Enriquez mineralization are trapped as isolated clusters and randomly distributed within the host quartz, thus suggesting a primary origin. A subordinate group of fluid inclusions occurs along healed fractures instead and can be therefore considered secondary in origin.

One dominant type of fluid inclusions is observed in quartz veins. This is represented by two-phase, liquid-rich (LV) at room temperature fluid inclusions (hereafter Type 1). Type 1 inclusions have been further divided in two subtypes: Type 1a and Type 1b based on their primary (Type 1a) and secondary (Type 1b) origin (Figures 10A, B). Both Type 1a and Type 1b fluid inclusions have an ellipsoidal shape but in several cases, they also show an irregular morphology, with the vapor bubble that fills 30%–40% of the total volume of the inclusions (Figures 10C, D). Type 1a inclusions are generally 5–15 μm in size, whereas Type 1b inclusions are smaller than Type 1a ranging between <5 μm and 10 μm in size.

4.3.1 Microthermometric results

The results of microthermometric investigation are summarized in Figures 10E, F. Type 1a and 1b fluid inclusions freeze to ice upon cooling below −40/−50°C. During warming, initial melting of ice (eutectic temperature T_e) was only measured in few Type 1a fluid inclusions and resulted around −25°C. This would suggest the occurrence of NaCl and KCl as main dissolved salts in the aqueous solution (Crawford, 1981); however, the paucity of T_e data gives a large margin of uncertainty to this conclusion. Type 1a fluid inclusions have a temperature of final ice melting (T_{mi}) between −0.4°C and −2.2°C with a mode at around −0.9°C, equating to salinities between 0.7 and 3.7 wt% $NaCl_{equiv}$. (mode at 1.5 wt% $NaCl_{equiv.}$). During heating runs, Type 1a fluid inclusions homogenized (T_h) into the liquid phase at temperatures between 326°C and 369°C with a mode around 345°C.

During cryometric experiments, no T_e data and only 5 T_{mi} data were obtained for Type 1b fluid inclusions due to their small size. The T_{mi} resulted in the range −0.6/−2.2°C, corresponding to salinities between 1.0 and 3.7 wt% $NaCl_{equiv.}$ Upon heating, these inclusions exhibit T_h ranging between 224°C and 323°C with a modal value at 305°C.

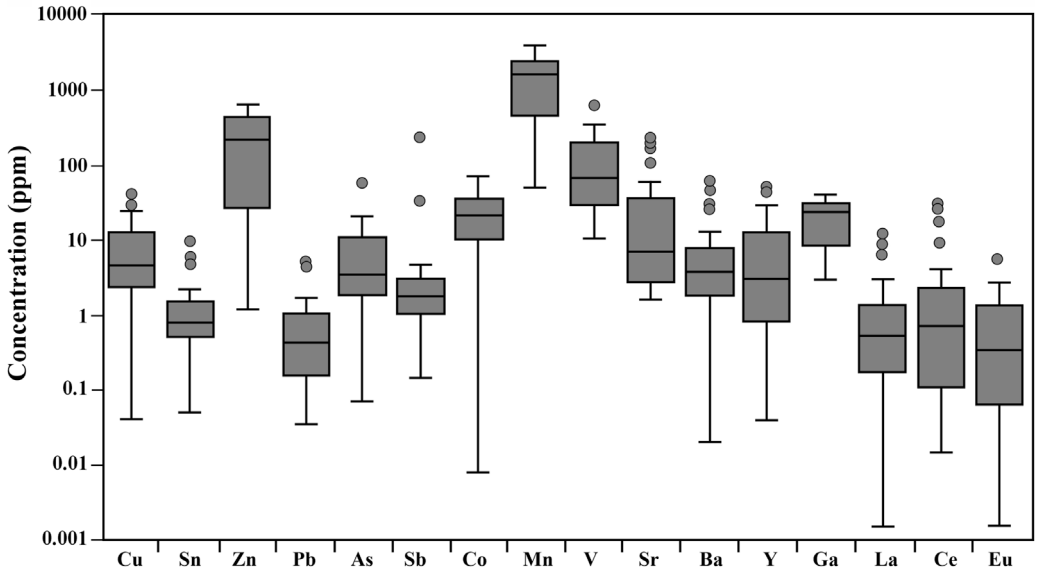

FIGURE 8
Summary of compositional ranges of selected minor and trace elements in chlorite from PEMD. Horizontal line represents median; box represents 25th to 75th percentiles, whiskers represent maximum and minimum excluding outliers; circles represent outliers. Data in Supplementary Material S1.

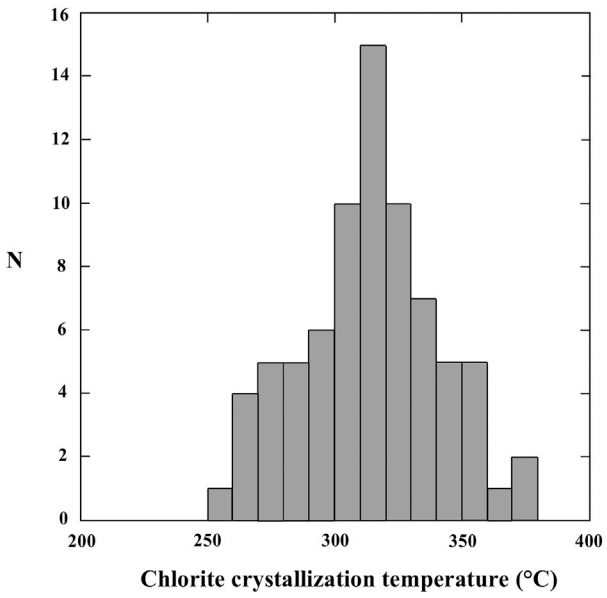

FIGURE 9
Histogram of the chlorite formation temperatures calculated with Cathelineau (1988); Jowett (1991) geothermometers (the differences between the two geothermometers are within ± 2°C).

5 Discussion

Despite the economic importance of the gold mineralization occurring in Southern Ecuador very little is known about the physical-chemical conditions of fluids that led to the formation of the hydrothermally altered rocks hosting the mineralization. This work aims to fill this gap, by using the PEMD as a case study for improving the general knowledge of the propylitically altered rocks in Ecuador and add new data for the use of trace element chemistry of epidote and chlorite in mineral exploration elsewhere.

In the PEMD, the pervasive hydrothermal alteration, mainly affected the mafic volcanic rocks of the Pallatanga Fm. and is composed of quartz, epidote, and chlorite, with subordinate amounts of illite, titanite and prehnite. This alteration assemblage may be similar to that of typical lower greenschist facies metamorphism (e.g., Turner, 1981). However, propylitic alteration, normally developed as an outer halo of many porphyries Cu-Au-Mo deposits (Lowell and Guilbert, 1970; Seedorf et al., 2005; Sillitoe, 2010), is similarly expressed by the same mineralogical assemblage (quartz, chlorite, epidote, prehnite). Recent papers demonstrated that the trace element content of epidote (particularly As and Sb content) can be used to discriminate epidote of metamorphic origin from epidote owing to propylitic alteration halo of porphyry copper deposits, and also between epidote from giant porphyry deposits and epidote from small porphyry deposits (Cooke et al., 2014; 2020a; b; Wilkinson et al., 2020). In particular, Cooke et al. (2020b) showed that epidote from the giant porphyry deposits is characterized by As and Sb contents that are one or more orders of magnitude greater than epidote from small porphyry deposits, whereas metamorphic epidote is characterized by very low As and Sb (commonly below detection limits; Baker et al., 2017). The high trace element and metal content of epidote from the propylitic halo of porphyry deposits has been attributed to the capacity of porphyry systems (large porphyry systems in particular) to flux metals, and this can be recorded in the trace element geochemistry of the distal propylitic alteration minerals (e.g., epidote), with greater distal pathfinder metal contents detected in epidote peripheral to larger deposits (Cooke et al., 2014). The As and Sb content of epidote analyzed in the altered mafic volcanic rocks of the Pallatanga Fm. fall in the field

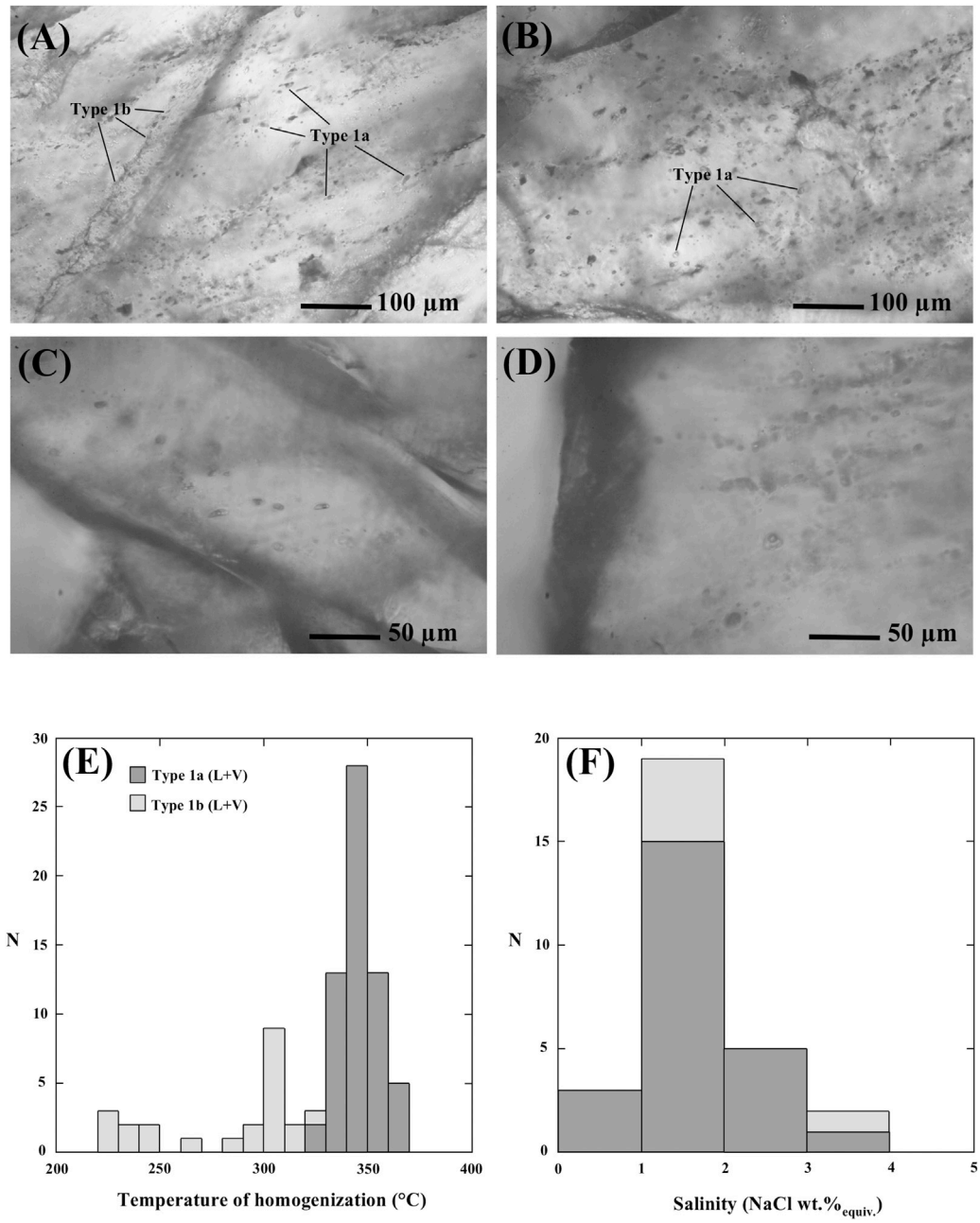

FIGURE 10
Microphotographs of fluid inclusions. **(A)** Primary two-phase liquid-rich (LV) fluid inclusions (Type 1a) and secondary trails of liquid-rich (LV) fluid inclusions (Type 1b). **(B)** Type 1a liquid-rich (LV) fluid inclusions. **(C,D)** Type 1a liquid-rich (LV) fluid inclusions showing ellipsoidal and, in some cases, irregular shapes. **(E)** Histogram of the homogenization temperatures of the analyzed fluid inclusions. **(F)** Histogram of the salinities of the analyzed fluid inclusions. N = number of measurements.

of porphyry deposits (Figure 11). This indicates that the pervasive alteration characteristic of mafic volcanic rocks of the Pallatanga Fm. can be related to the propylitic alteration halo of porphyry copper deposits. Most of the As and Sb data on epidotes plots in the lower left part of the porphyry data field (Figure 11) and therefore could be interpreted as epidote collected from either close to a giant porphyry deposit or distal to a small porphyry deposit. The coexistence of pyrite with epidote must also be considered, since As and Sb are more likely to be incorporated into pyrite than epidote when these minerals co-precipitate (Cooke et al., 2014; 2020a; b). In our case there is no evidence of the constant coexistence of epidote and pyrite, as a consequence we consider more realistic the second interpretation, i.e., distal to a small porphyry deposit.

Fluid inclusion data support the interpretation of propylitic hydrothermal alteration linked to porphyry systems for the "green rocks" associated with PEMD. Indeed, fluid inclusions in quartz veins associated with epidote and chlorite show that the fluid circulated in the mafic volcanic rocks of Pallatanga Fm. had low

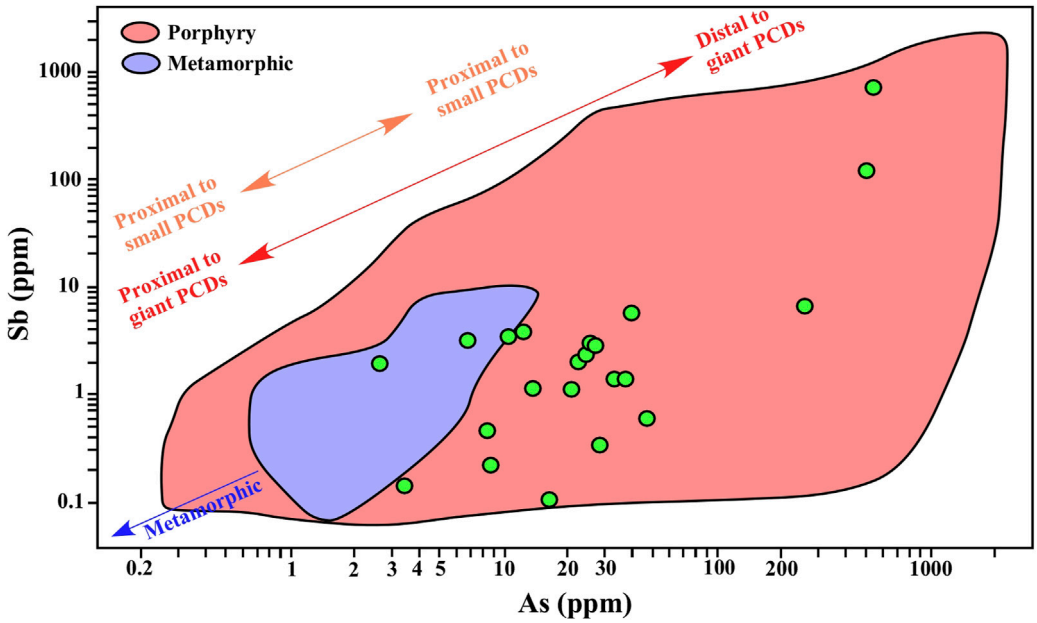

FIGURE 11
As-Sb LA-ICPMS data of PEMD epidotes (data in Supplementary Material S1) compared with epidote composition from propylitic halo of porphyry deposits and from metamorphic rocks. The As-Sb fields of epidotes from porphyry deposits and metamorphic epidotes are from Cooke et al. (2020b) and references therein.

salinity (around 1.5 wt% $NaCl_{equiv.}$) suggesting a meteoric origin and temperatures between 300°C and 350°C. These data are basically consistent with the conditions of propylitic alteration formation of porphyry-type deposits (Seedorf et al., 2005; Sillitoe, 2010; Ni et al., 2015; Li et al., 2017) and are also typical of the propylitic alteration found in several active hydrothermal systems (Bird et al., 1984; Reyes, 1990; Berger and Velde, 1992). At least two pulses of hydrothermal fluids have been recognized thanks to fluid inclusions: the first one (probably responsible for the main development of propylitic alteration) characterized by temperature around 345°C, the second one with temperature around 305°C, indicating the cooling of the hydrothermal fluids. The lower temperature event corresponds quite well to the modal value of the temperature calculated by chlorite geothermometers (around 315°C, Figure 9). This suggests that chlorite composition may have re-equilibrated with the temperature conditions characteristics of the second and relatively lower temperature fluid. However, assuming a possible error of at least ±30°C for chlorite geothermometry (Fulignati, 2020 and reference therein), it is difficult to discriminate between the two hydrothermal pulses. The temperatures estimated with chlorite geothermometers are basically in the range of the homogenization temperatures measured in fluid inclusions in quartz associated with the PEMD propylitic alteration. This indicates that these homogenization temperatures can be probably considered as representing the true trapping temperature of the fluids, and pressure correction is not required. This also means that propylitic alteration in PEMD developed at relatively low-pressure conditions (below 10–20 MPa) probably under hydrostatic regime, suggesting a shallow depth environment. Fluid inclusion data did not reveal any evidence of boiling processes.

Taking into account the above considerations and the geological context of the area, we hypothesize that PEMD hydrothermally altered rocks could be envisaged as the propylitic halo of the Miocene hornblende-bearing Au-Cu porphyry deposits of Gaby-Papa Grande (Schutte et al., 2012). The application of chlorite proximitor (Wilkinson et al., 2015) gave a calculated distance from the collected samples to the causative porphyry systems ranging between 1,300 and 1,600 m, which may be plausible for Gaby-Papa Grande (Figure 1).

The improved knowledge of the propylitic alteration affecting the Pallatanga mafic volcanics can be useful for interpreting rock alteration and discriminate porphyry-related propylitic style during mineral exploration in this region, as well as elsewhere. An open question concerns the relationships existing between the vein gold mineralization and the propylitic alteration event. Are they coeval or not? To shed light on these topics, pivotal for the comprehension of the Ponce Enriquez gold mineralization genesis, further research has to be addressed to carry out dating data on the mineralization and propylitic alteration mineralogical assemblages.

6 Conclusion

This work, for the first time, tackles the study of propylitic alteration in the Ponce Enriquez mining district (Southern Ecuador) as a case study to improve understanding of the formation of propylitically altered rocks and their possible use as a mineral exploration tool. The investigation of these “green rocks” is particularly relevant because they host a significant gold mineralization, exploited in the last decades. The main conclusions of the study are as follow:

- The mafic volcanic rocks of the Pallatanga Fm. are affected by a pervasive alteration characterized by a mineralogical assemblage formed by chlorite + epidote + quartz + titanite ± illite ± prehnite ± calcite.
- The As and Sb content of epidote from these "green rocks" indicates that the alteration characteristic of mafic volcanic rocks of the Pallatanga Fm. can be related to the propylitic hydrothermal alteration halo of porphyry copper deposits.
- At least two pulses of hydrothermal fluid circulation have been recognized (the first one at T = 345°C, the second one at T = 305°C) thanks to the study of fluid inclusions hosted in quartz veins associated with epidote and chlorite.
- The salinity of the fluids is always low (around 1.5 wt% $NaCl_{equiv.}$) suggesting a dominantly meteoric component. No boiling evidence has been observed.
- The trace element contents of propylitic alteration minerals help to indicate that PEMD hydrothermally altered rocks could be envisaged as the propylitic halo of the Miocene hornblende-bearing Au-Cu porphyry deposits of Gaby-Papa Grande.

The results of this paper represent the first pieces of the puzzle concerning the PEMD mineralization. These, integrated and corroborated with further analytical studies, will help in defining a conceptual working model for the Ecuadorian gold endowment. This will be useful in the mineral exploration of the Azuay and El Oro Provinces of Ecuador, where several gold mineralizations occur in a general context similar to PEMD, and also in other regions worldwide where gold mineralization occur associated to propylitic alteration facies.

This work furthermore confirms that trace element analysis of epidote and chlorite, coupled with other methods of investigation (i.e., fluid inclusion data), is a powerful tool in mineral exploration, being able to discriminate between propylitic hydrothermal alteration halos formed by porphyry systems from similar mineral assemblages formed through regional metamorphic processes.

Data availability statement

The original contributions presented in the study are included in the article/Supplementary Material, further inquiries can be directed to the corresponding authors.

Author contributions

PF: Conceptualization, Data curation, Project administration, Validation, Writing–original draft. MMu: Conceptualization, Data curation, Project administration, Validation, Writing–original draft. MV: Data curation, Methodology, Writing–original draft. SF: Writing–review and editing. EL: Data curation, Writing–review and editing. PM: Data curation, Methodology, Writing–review and editing. MMe: Data curation, Methodology, Writing–review and editing. PR-C: Conceptualization, Project administration, Writing–review and editing. AG: Conceptualization, Data curation, Project administration, Validation, Writing–original draft.

Funding

The project was partially funded by the ERASMUS+ KA107 European Project 2019 University of Pisa-ESPOL that permitted the research stays. The field activities were funded with the support of the FICT and the ESPOL research deanery research funds. Analytical data were funded by University of Pisa "Fondi d'Ateneo 2022" to AG and by University of Pisa "PRA Progetti di Ricerca di Ateneo, Project no. PRA_2022-2023_66" to PF.

Acknowledgments

We thank Richard Torres and the Bella Rica Mining Cooperative for permitting and supporting the sampling process. We kindly appreciate the help of Nancy Zumba, Victoria Rosado, Valeria Vaca, and Andrei Zambrano for the thin sections. We also wish to warmly thank Randa Ishak and Andrea Risplendente for the precious help with FE-SEM-EDS and EPMA analysis respectively. A particular thank is due to Matteo Masotta for his friendly and essential assistance during analytical work and data reduction of LA-ICPMS data. We finally thank four reviewers whose comments and suggestions helped to improve the quality and the clarity of the present manuscript. The manuscript benefited of the editorial handling of Prof Ryan Mathur.

Conflict of interest

The authors declare that the research was conducted in the absence of any commercial or financial relationships that could be construed as a potential conflict of interest.

Publisher's note

Supplementary material

The Supplementary Material for this article can be found online at: https://www.frontiersin.org/articles/10.3389/feart.2023.1255712/full#supplementary-material

References

Ahmed, A. D., Fisher, L., Pearce, M., Escolme, A., Cooke, D. R., Howard, D., et al. (2020). A microscale analysis of hydrothermal epidote: implications for the use of laser ablation-inductively coupled plasma-mass spectrometry mineral chemistry in complex alteration environments. *Econ. Geol.* 115, 793–811. doi:10.5382/econgeo.4705

AMBIENCONSUL (2017). *Estudio de impacto ambiental y plan de manejo ambiental exposto para la fase de explotación y beneficio de minerales metálicos bajo el régimen de pequeña minería de las concesiones mineras Bella Rica y Guanache-Tres de Mayo*. (in Spanish). Technical report.

Appleton, J. D., Williams, T. M., Orbea, H., and Carrasco, M. (2001). Fluvial contamination associated with artisanal gold mining in the Ponce Enriquez, Portovelo-Zaruma and Nambija areas, Ecuador. *Water Air Soil Poll.* 131, 19–39. doi:10.1023/A:1011965430757

Baker, M., Cooke, D. R., Hollings, P. N., and Piquer, J. (2017). "Identification of hydrothermal alteration related to mineralisation using epidote mineral chemistry," in Proceedings of the 14th SGA Biennial Meeting: Mineral Resources to Discover, Québec City, Canada, August 2017.

Baker, M., Wilkinson, J. J., Wilkinson, C. C., Cooke, D. R., and Ireland, T. (2020). Epidote trace element chemistry as an exploration tool in the Collahuasi District, Northern Chile. *Econ. Geol.* 115, 749–770. doi:10.5382/econgeo.4739

Berger, G., and Velde, B. (1992). Chemical parameters controlling the propylitic and argillic alteration process. *Eur. J. Mineral.* 4, 1439–1456. doi:10.1127/ejm/4/6/1439

Bettison, L. A., and Schiffman, P. (1988). Compositional and structural variations of phyllosilicates from the Point Sal ophiolite, California. *Am. Mineral.* 73 (1-2), 62–76.

Bird, D. K., Schiffman, P., Elders, W. A., Williams, A. E., and McDowell, S. D. (1984). Calc-silicate mineralization in active geothermal systems. *Econ. Geol.* 79 (4), 671–695. doi:10.2113/gsecongeo.79.4.671

Bodnar, R. J. (1993). Revised equation and table for determining the freezing point depression of H_2O-NaCl solutions. *Geochim. Cosmochim. Acta* 57, 683–684. doi:10.1016/0016-7037(93)90378-a

Boyce, A. J., Fulignati, P., and Sbrana, A. (2003). Deep hydrothermal circulation in a granite intrusion beneath larderello geothermal area (Italy): constraints from mineralogy, fluid inclusions and stable isotopes. *J. Volcanol. Geotherm. Res.* 126, 243–262. doi:10.1016/S0377-0273(03)00150-1

Carling, G. T., Diaz, X., Ponce, M., Perez, L., Nasimba, L., Pazmino, E., et al. (2013). Particulate and dissolved trace element concentrations in three southern Ecuador rivers impacted by artisanal gold mining. *Water Air Soil Poll.* 224, 1415–1416. doi:10.1007/s11270-012-1415-y

Cathelineau, M. (1988). Cation site occupancy in chlorites and illites as a function of temperature. *Clay Min.* 23 (4), 471–485. doi:10.1180/claymin.1988.023.4.13

Cavarretta, G., Gianelli, G., and Puxeddu, M. (1982). Formation of authigenic minerals and their use as indicators of the physicochemical parameters of the fluid in the Larderello-Travale geothermal field. *Econ. Geol.* 77 (5), 1071–1084. doi:10.2113/gsecongeo.77.5.1071

Cooke, D. R., Agnew, P., Hollings, P., Baker, M., Chang, Z., Wilkinson, J. J., et al. (2020a). Recent advances in the application of mineral chemistry to exploration for porphyry copper–gold molybdenum deposits: detecting the geochemical fingerprints and footprints of hypogene mineralization and alteration. *Geochem. Expl. Env. An.* 20, 176–188. doi:10.1144/geochem2019-039

Cooke, D. R., Baker, M., Hollings, P., Sweet, G., Chang, Z., Danyushevsky, L., et al. (2014). New advances in detecting the distal geochemical footprints of porphyry systems: epidote mineral chemistry as a tool for vectoring and fertility assessments. *Soc. Econ. Geol. Spec. Publ.* 18, 127–152. doi:10.5382/SP.18.07

Cooke, D. R., Wilkinson, J. J., Baker, M., Agnew, P., Phillips, J., Chang, Z., et al. (2020b). Using mineral chemistry to aid exploration: A case study from the resolution porphyry Cu-Mo deposit, Arizona. *Econ. Geol.* 115, 813–840. doi:10.5382/econgeo.4735

Crawford, M. L. (1981). "Phase equilibria in aqueous fluid inclusions,". *Short course in fluid inclusions: Application to petrology*. Editors L. S. Hollister and M. L. Crawford (Canada: Mineralogical Association of Canada), 75–100.

Dunkley, P. N., and Gaibor, A. (1997). *Informe N° 2, proyecto de Desarrollo minero y control ambiental, programa de Información cartográfica y geológica: Geology of the western Cordillera of Ecuador between 2-3°S*. Quito, Ecuador: CODIGEM-BGS. (In Spanish).

Duque, P. (2000). *Breve Léxico estratigráfico del Ecuador*. Quito: UCP PRODEMINCA. (In Spanish).

Egüez, A., Gaona, M., and Albán, A. (2017). *Mapa Geológico de la República del Ecuador escala 1:1000000*. Quito, Pichincha: Instituto Nacional de Investigación Geológico Minero Metalúrgico. (In Spanish).

Fulignati, P. (2020). Clay minerals in hydrothermal systems. *Minerals* 10 (10), 919. doi:10.3390/min10100919

Goldstein, R. H., and Reynolds, T. J. (1994). Systematics of fluid inclusions in diagenetic minerals. *Soc. Sediment. Geol. Short Course* 31, 199. doi:10.2110/scn.94.31

Hastie, A. R., Kerr, A. C., Pearce, J. A., and Mitchell, S. F. (2007). Classification of altered volcanic island arc rocks using immobile trace elements: development of the Th-Co discrimination diagram. *J. Petrol.* 48, 2341–2357. doi:10.1093/petrology/egm062

Hungerbuhler, D. (1997). *Tertiary basins in the andes of southern Ecuador (3°00′–4°20′): Sedimentary evolution, deformation and regional tectonic implications*. PhD Thesis,Hyderabad: Institute of Geology,

Jiménez-Oyola, S., Chavez, E., García-Martínez, M. J., Ortega, M. F., Bolonio, D., Guzmán-Martínez, F., et al. (2021a). Probabilistic multi-pathway human health risk assessment due to heavy metal (loid) s in a traditional gold mining area in Ecuador. *Ecotox Environ. Safe.* 224, 112629. doi:10.1016/j.ecoenv.2021.112629

Jiménez-Oyola, S., García-Martínez, M. J., Ortega, M. F., Chavez, E., Romero, P., García-Garizabal, I., et al. (2021b). Ecological and probabilistic human health risk assessment of heavy metal (loid) s in river sediments affected by mining activities in Ecuador. *Environ. Geochem. Health* 43 (11), 4459–4474. doi:10.1007/s10653-021-00935-w

Jowett, E. C. (1991). "Fitting iron and magnesium into the hydrothermal chlorite geothermometer," in Proceedings of the Geological Association of Canada + MAC + SEG Joint Annual MeetingAt: Toronto ONVolume: Program, Toronto, May 27–29, 1991, A62.

Kerr, A. C., Aspden, J. A., Tarney, J., and Pilatasig, L. F. (2002). The nature and provenance of accreted oceanic terranes in western Ecuador: geochemical and tectonic constraints. *J. Geol. Soc. Lond.* 159 (5), 577–594. doi:10.1144/0016-764901-151

Le Bas, M. J., Le Maitre, R. W., Steckeisen, A., and Zanettin, B. (1986). A chemical classification of volcanic rocks based on the total alkali-silica diagram. *J. Petrol.* 27, 745–750. doi:10.1093/petrology/27.3.745

Li, C., Shen, P., Li, P., Sun, J., Feng, H., and Pan, H. (2022). Changes in the factors controlling the chlorite composition and their influence on hydrothermal deposit studies: A case study from hongguleleng manto-type Cu deposit. *J. Geochem. Explor.* 243, 107096. doi:10.1016/j.gexplo.2022.107096

Li, L., Ni, P., Wang, G.-G., Zhu, A.-D., Pan, J.-Y., Chen, H., et al. (2017). Multi-stage fluid boiling and formation of the giant Fujiawu porphyry Cu–Mo deposit in South China. *Ore Geol. Rev.* 81, 898–911. doi:10.1016/j.oregeorev.2015.11.020

Lowell, J. D., and Guilbert, J. M. (1970). Lateral and vertical alteration-mineralization zoning in porphyry ore deposits. *Econ. Geol.* 65 (4), 373–408. doi:10.2113/gsecongeo.65.4.373

Ni, P., Wang, G.-G., Yu, W., Chen, H., Jiang, L.-L., Wang, B.-H., et al. (2015). Evidence of fluid inclusions for two stages of fluid boiling in the formation of the giant Shapinggou porphyry Mo deposit, Dabie Orogen, Central China. *Ore Geol. Rev.* 65, 1078–1094. doi:10.1016/j.oregeorev.2014.09.017

Pacey, A., Wilkinson, J. J., and Cooke, D. R. (2020). Chlorite and epidote mineral chemistry in porphyry ore systems: A case study of the northparkes district, new south wales, Australia. *Econ. Geol.* 115, 701–727. doi:10.5382/econgeo.4700

Paton, C., Hellstrom, J., Paul, B., Woodhead, J., and Hergt, J. (2011). Iolite: freeware for the visualisation and processing of mass spectrometric data. *J. Anal. At. Spectr.* 26, 2508. doi:10.1039/c1ja10172b

Pesantes, A. A., Carpio, E. P., Vitvar, T., López, M. M. M., and Menéndez-Aguado, J. M. (2019). A multi-index analysis approach to heavy metal pollution assessment in river sediments in the Ponce Enríquez Area, Ecuador. *Water* 11 (3), 590. doi:10.3390/w11030590

Pratt, W., Figueroa, J., and Flores, B. (1997). *Informe N° 1, proyecto de Desarrollo minero y control ambiental, programa de Información cartográfica y geológica: Geology and mineral deposits of the western Cordillera of Ecuador between 3-4° S*. Quito, Ecuador: CODIGEM-BGS. (In Spanish).

PRODEMINCA (2000). Evaluación de distritos mineros del Ecuador: depósitos porfídicos y epi-mesotermales relacionados con intrusiones de las cordilleras Occidental y real. *UCP PRODEMINCA Proy. Mem. BIRF, EC, Quito* 4, 36–55. (In Spanish).

Reyes, A. G. (1990). Petrology of Philippine geothermal systems and the application of alteration mineralogy to their assessment. *J. Volcanol. Geotherm. Res.* 43 (1-4), 279–309. doi:10.1016/0377-0273(90)90057-M

Schütte, P., Chiaradia, M., Barra, F., Villagómez, D., and Beate, B. (2012). Metallogenic features of Miocene porphyry Cu and porphyry-related mineral deposits in Ecuador revealed by Re-Os, 40Ar/39Ar, and U-Pb geochronology. *Min. Deposita* 47 (4), 383–410. doi:10.1007/s00126-011-0378-z

Seedorff, E., Dilles, J. H., Proffett, J. M., Einaudi, M. T., Zurcher, L., Stavast, W. J., et al. (2005). Porphyry deposits: characteristics and origin of hypogene features. *Econ. Geol.* 100, 251–298. doi:10.5382/AV100.10

Sillitoe, R. H. (2010). Porphyry copper systems. *Econ. Geol.* 105 (1), 3–41. doi:10.2113/gsecongeo.105.1.3

Siravo, G., Speranza, F., Mulas, M., and Costanzo-Alvarez, V. (2021). Significance of northern andes terrane extrusion and genesis of the interandean valley: paleomagnetic evidence from the "Ecuadorian orocline". *Tectonics* 40, e2020TC006684. doi:10.1029/2020TC006684

Srivastava, M., Steidtmann, H., and Gowans, R. M. (2008). NI 43–101 Technical report on the preliminary feasibility study for the Gaby gold project, Ecuador. Available at: http://www.sedar.com. Accessed 26 May 2009

Thalmann, H. (1946). Micropaleontology of upper cretaceous and paleocene in western Ecuador. *AAPG Bull.* 30 (3), 337–347. doi:10.1306/3D933802-16B1-11D7-8645000102C1865D

Turner, F. J. (1981). *Metamorphic petrology*. New York: McGraw Hill.

Wilkinson, J. J., Baker, M. J., Cooke, D. R., and Wilkinson, C. C. (2020). Exploration targeting in porphyry Cu systems using propylitic mineral chemistry: A case study of the El Teniente deposit, Chile. *Econ. Geol.* 115, 771–791. doi:10.5382/econgeo.4738

Wilkinson, J. J., Chang, Z., Cooke, D. R., Baker, M. J., Wilkinson, C. C., Inglis, S., et al. (2015). The chlorite proximitor: A new tool for detecting porphyry ore deposits. *J. Geochem. Explor.* 152, 10–26. doi:10.1016/j.gexplo.2015.01.005